Bifurcation and Relaxation of Radial Electric Field in Enhanced Reversed Shear Tokamak Plasmas

K. C. Shaing,[1] A. Y. Aydemir,[1] R. Hiwatari,[2] W. A. Houlberg,[3] Y. Ogawa,[2] and M. C. Zarnstorff[4]
[1]*Institute for Fusion Studies, The University of Texas, Austin, Texas 78712*
[2]*School of Engineering, University of Tokyo, Tokyo, Japan*
[3]*Oak Ridge National Laboratory, Oak Ridge, Tennessee 37831*
[4]*Princeton Plasma Physics Laboratory, Princeton, New Jersey 08543*
(Received 27 April 1999)

It is shown that toroidal magnetic field ripple induced thermal and fast ion loss can drive the radial electric field to bifurcate over the local maximum of the parallel (or poloidal) viscosity. The subsequent plasma profile evolution reduces the hot particle density and relaxes the radial electric field. This behavior is consistent with the experimental observations in enhanced reversed shear mode in tokamaks.

PACS numbers: 52.55.Fa, 52.25.Dg, 52.25.Fi

To make an economical nuclear fusion reactor, it is necessary to improve its plasma confinement property. An improved confinement mode (i.e., H mode) in the edge region of a tokamak and a stellarator was observed [1–3]. The mechanism for the confinement improvement is due to the bifurcation of the radial electric field E_r and the subsequent turbulence suppression due to the radial gradients of the $\mathbf{E} \times \mathbf{B}$ and the diamagnetic angular velocity [4–6]. Here, $\mathbf{E}$ is the electric field and $\mathbf{B}$ is the magnetic field.

Recently, the improved confinement modes in the core region were also observed [7–9]. There are two basic types of the core confinement improvement modes. One is the enhanced reversed shear (ERS) mode [7,8], and the other is the negative central shear (NCS) mode [9]. Both of these phenomena can be explained by the same mechanism that triggers the improved edge confinement mode. Although the magnetic shear is reversed in both modes, i.e., the radial gradient of the safety factor q is positive in the region close to the magnetic axis, the mechanisms that generate E_r are quite different. In the NCS mode, E_r is generated by the toroidal rotation associated with the unidirectional neutral particle beam momentum injection. In the ERS mode, however, the unidirectional neutral particle beam momentum is negligible. It is observed experimentally that in the ERS-mode poloidal plasma rotation suddenly increases (or bifurcates) to a large value and subsequently relaxes in the transport time scale [10,11]. The magnitude of the poloidal rotation excursion in terms of the poloidal Mach number is of the order of unity. While the E_r profile in the NCS mode can be easily explained by the toroidal momentum input associated with the neutral particle beam injection, the bifurcation and relaxation of E_r in the ERS mode cannot be easily explained. Here, we advance a theory to explain such an important phenomenon without resorting to unquantifiable parameters.

Note that it is quite unusual that in the relaxation process there is no back bifurcation involved in the ERS mode. Thus, the parameter-dependent nonlinearity in our theory may serve as a paradigm for other similar nonlinear phenomena in nature as well.

It has been shown that toroidal magnetic field ripple induced particle fluxes can drive the radial electric field E_r to bifurcate over the local maximum of the poloidal (or parallel) viscosity [12]. This mechanism provides an explanation for the bifurcation of E_r observed in ERS mode in tokamaks. The radial electric field, however, relaxes in a few hundred ms after the bifurcation [10,11]. To explain this relaxation phenomenon, either the rippled induced ion loss has to decrease or the electron loss has to increase or a combination of both. While there are magnetohydrodynamic (MHD) activities observed after the bifurcation [10], it is difficult to quantify the particle loss associated with this MHD activity unambiguously. It would be better if a theory can be developed based on the reduction of the ion ripple loss after bifurcation to explain the relaxation phenomenon. The reason is that ion ripple loss can be more accurately determined than electron loss resulting from MHD activities.

Here, we demonstrate the relaxation of E_r by including both thermal and fast ion ripple losses. Fast ion ripple loss assists bifurcation. After bifurcation, plasma confinement improves and thermal ion density increases. The increase of the thermal ion density makes it harder to neutral beam particles to penetrate. Fast ion density and its ripple loss are therefore reduced after the bifurcation. The radial electric field is then relaxed. This mechanism seems to be applicable for the ERS mode observed in Tokamak Fusion Test Reactor (TFTR) [2].

There is another mechanism for the reduction of ion ripple loss after the bifurcation. It is possible in some devices that ion ripple loss is dominated either by the ripple trapping [13] or by the banana drift [14–17]. Ripple trapping loss mechanism is associated with collisionless particles that are trapped in the magnetic well created by the toroidal magnetic field ripple. These particles drift off the magnetic surface and cause local particle loss. The banana drift loss mechanism results from the particles that are trapped in the toroidal magnetic well. Because

 0031-9007/99/83(19)/3840(4)$15.00

toroidal magnetic field ripple breaks toroidal symmetry, the bounce trajectory of these particles is not closed. This also leads to local particle loss. Both of these loss mechanisms are present in collisionless rippled tokamaks. As ion temperature increases, ion ripple loss could increase first which drives bifurcation of E_r and then reduces to relax E_r if the effective collision frequency is, at the beginning, larger than the $\mathbf{E} \times \mathbf{B}$ drift frequency of the ripple trapped ions or banana drifting ions and then later becomes smaller than the drift frequency. For TFTR plasma parameters, this mechanism may not be applicable. However, it could be operative in other devices.

We emphasize that the details in determining E_r may vary from device to device. However, extended neoclassical theory that takes the details of the experimental operation into account should be able to determine E_r with reasonable accuracy [4,18].

For simplicity, we assume only that poloidal Mach number due to $\mathbf{E} \times \mathbf{B}$ rotation is of the order of the ion thermal speed, i.e., $M_{pE} = cE_r/(B_p v_{ti}) \sim 1$ where c is the speed of light, B_p is the poloidal magnetic field strength, and v_{ti} is the ion thermal speed. The Mach number of the poloidal flow V_θ is assumed to be less than unity, i.e., $M_{p\theta} = V_\theta B/(B_p v_{ti}) < 1$ where $B = |\mathbf{B}|$. With this assumption the plasma compressibility effects, such as shock formation, can be neglected. It has been demonstrated that qualitative bifurcation behavior is not affected by the compressibility effects. Because $M_{p\theta} < 1$, the convective $\mathbf{V} \cdot \nabla \mathbf{V}$ term in the fluid momentum can be neglected. Here, $\mathbf{V}$ is the plasma flow velocity. We note that the compressibility effects that result from $V_\theta B/(B_p v_{ti}) \sim 1$ are intrinsically nonlinear phenomena of the nondissipative momentum equation and cannot be correctly described by the solution of the drift kinetic equation.

The steady toroidal and poloidal momentum balance equations are [12]

$$\langle \mathbf{B}_t \cdot \nabla \cdot \Sigma_a \Pi_a \rangle = \langle \mathbf{B}_t \cdot \Sigma_a \mathbf{S}_{ma} \rangle , \tag{1}$$

$$\langle \mathbf{B}_p \cdot \nabla \cdot \Sigma_a \Pi_a \rangle = 0 , \tag{2}$$

where $\mathbf{B}_t$ is the toroidal magnetic field, Π_a is the viscous tensor of species a, $\mathbf{S}_{ma}$ is the momentum source, and the angular brackets denote flux surface average. For simplicity, we neglect the toroidal momentum source term in Eq. (1).

For the plasma parameters in current devices, the important ripple loss mechanisms are ripple trapping, banana drift, and collisionless ripple plateau [19]. Because the leading order perturbed particle distribution function for these loss mechanisms has no variation along the magnetic line, $\langle \mathbf{B}_p \cdot \nabla \cdot \Pi_a \rangle = -\langle \mathbf{B}_t \cdot \nabla \cdot \Pi_a \rangle = -(e_a B_p B \Gamma_r^a / c)$, where Γ_r^a is the ripple induced flux and e_a is charge [20]. The ripple trapping flux for species a is [19]

$$\Gamma_t^a = -\, 0.018 n_a \frac{1}{\alpha^3} \left(\frac{cT_a}{e_a B R} \right)^2 \frac{1}{\delta^{1/2}} \times \int dx\, \nu_a x^6 e^{-x^2} \times \frac{p_a'/p_a + e_a \Phi'/T_a + (x^2 - 5/2) T_a'/T_a}{\alpha^2 (\frac{cT_a}{e_a B R r} x^2 + \frac{cE_r}{Br})^2 + (\nu_a/\delta)^2} , \tag{3}$$

where $\alpha = \epsilon/(Nq\delta)$, $\epsilon = r/R$, r is the minor radius, R is the major radius, N is the number of the toroidal magnetic field coils, δ is the ripple well depth, ν_a is the collision frequency, p_a is the plasma pressure, T_a is the temperature, n_a is the plasma density, and prime denotes d/dr. Note that to obtain Eq. (3) we have assumed $\alpha > 1$. The banana drift flux is [19]

$$\Gamma_b^a = -\, \frac{0.15 n_a N q R^2 \delta^2}{\sqrt{2\pi\epsilon}} \int_{(W_p/T_a)^2}^{\infty} dx\, x^6 e^{-x^2} (\nu_a \rho_{pa}^2 / 4R^2) \times \frac{P_a'/P_a + e_a \Phi'/T_a + (x^2 - 5/2) T_a'/T_a}{(\frac{cE_r}{B_p v_{ta}} + \tilde{Q} \frac{\rho_{pa} x^2}{2R})^2 + 0.4 (\frac{cE_r}{B_p v_{ta}} + \tilde{Q} \frac{\rho_{pa} x^2}{2R}) (\frac{Nq\nu_a}{v_{ta}\epsilon/Rq}) + 0.2 (\frac{Nq\nu_a}{v_{ta}\epsilon/Rq})^2} , \tag{4}$$

where $\tilde{Q} = (1.5 d \ln q/d \ln r + 0.7)$, ρ_{pa} is the poloidal gyroradius, $v_{ta} = \sqrt{2T_a/M_a}$ is the thermal speed, M_a is the mass, $W_{pa}/T_a = (\nu_{*a} N^2 q^2)^{1/2}$, and $\nu_{*a} = (\nu_a R q / v_{ta} \epsilon^{3/2})$. The collisionless ripple plateau flux is [19]

$$\Gamma_{rp}^a = -\frac{n_a \delta_0^2 x_{Rp}^a}{6 \langle \delta^2 \rangle} \left[I_1 \left(\frac{P_a'}{P_a} + \frac{e_a \Phi'}{T_a} \right) + I_2 \frac{T_a'}{T_a} \right], \tag{5}$$

where $x_{Rp}^a = (3\sqrt{\pi}/4)(v_{ta}/Rq) \rho_{pa}^2 Nq \langle \delta^2 \rangle$, $\langle \delta^2 \rangle = \int_0^{2\pi} d\theta\, \delta^2/2\pi$, $I_1 = 2 \int_0^{(W_p^a/T_a)^{1/2}} dx\, e^{-x^2} x^5$, and $I_2 = 2 \int_0^{(W_p^a/T_a)^{1/2}} dx\, x^5 e^{-x^2} (x^2 - \frac{5}{2})$. We are interested in plasmas that consist of thermal ions ($a = i$), fast ions ($a = H$), and thermal electrons ($a = e$). For each of these species, there is a corresponding Γ_t^a, Γ_b^a, and Γ_{rp}^a. During the bifurcation and relaxation processes, ion temperatures, ion densities, and their gradients evolve. These quantities become part of the controlling parameters in the ERS mode transition.

The nonlinear resonant plasma viscosity due to banana and circulating particles is [21]

$$\langle \mathbf{B} \cdot \nabla \cdot \Pi_a \rangle_n = n_a M_a B^2 \left(\mu_{1a} U_{\theta a} + \frac{2}{5} \mu_{2a} \frac{q_{\theta a}}{\rho_a} \right), \tag{6}$$

where $U_{\theta a} = (v_{ta}/B)[V_\lambda/v_{ta} - cE_r/(B_p v_{ta}) + cP_a'/(n_a e_a v_{ta} B_p)]$ and $q_{\theta a}/p_a = (v_{ta}/B)[q_\lambda/(p_a v_{ta}) + \frac{5}{2} cT_a/(e_a v_{ta} B_p)]$. Because $V_{\|e} \approx V_{\|i} \ll v_{te}$ and $cE_r/(B_p v_{te}) \ll 1$, electron viscosity is not affected

in the regime where $cE_r/(B_p v_{ti}) \sim 1$, and standard electron viscosity coefficients apply. The ion nonlinear resonant viscosity coefficients in the banana regime are $(\kappa_{b1}, \kappa_{b2}) = \int_{|U_{pm}|}^{\infty} dx\, x^4 e^{-x^2} K_B(1, x^2)$, and in the plateau-Pfirsch-Schlüter regime they are $(\kappa_{ps1}, \kappa_{ps2}) = \int_0^{\infty} dx\, x^4 e^{-x^2} K_{ps}(1, x^2)$, where $K_{ps} = (\nu_i \epsilon^2/2\sqrt{\pi}) \int_{-1}^{1} dy\, (1-3y^2)(\nu_{*i} x/\nu_i)\{(y + U_{pm}/x)^2 + [\nu_{*i}\epsilon^{3/2}\nu_T(x)/\nu_i x]^2\}$, $\nu_T = 3\nu_D + \nu_E$ is the anisotropy relaxation frequency, $K_B = 1.46\sqrt{\epsilon}\,\nu_D(8/3\sqrt{\pi})(1 - 3U_{pm}^2/x^2)\mathbb{F}(1 + U_{pm}^2/x^2)^{-3/2}$, $\mathbb{F} = (1 - U_{pm}^2/x^2) + (\nu_\parallel/\nu_D)U_{pm}^2/x^2$, $U_{pm} = [V_{\parallel i}/v_{ti} - cE_r/(v_{ti}B_p)]$, and ν_D, ν_E, and $\nu_\parallel$ are defined in Ref. [22]. The nonlinear viscous coefficients are $\mu_{1a} = \kappa_{b1}^a \kappa_{ps1}^a/(\kappa_{b1}^a + \kappa_{ps1}^a)$ and $\mu_{2a} = \kappa_{b2}^a \kappa_{ps2}^a/(\kappa_{b2}^a + \kappa_{ps2}^a) - \frac{5}{2}\mu_{1a}$.

A dimensionless nonlinear equation for $M_p = -cE_r/(B_p v_{ti})$ can be derived by substituting Eqs. (3)–(6) into Eq. (2) to obtain

$$\frac{M_i \mu_{1i}}{M_e \mu_{1e}}\left(U_{pm} + \overline{c}_{pi} + \frac{\mu_{2i}}{\mu_{1i}}\overline{c}_{Ti}\right) = -U_{pm} - \overline{B} - D_i(\overline{c}_{pi} + M_p + R_i \overline{c}_{Ti}) - D_H\left(\overline{c}_{ph} + M_p\sqrt{\frac{T_i}{T_H}} + R_H \overline{c}_{TH}\right) + D_e\left(\overline{c}_{pe} - M_p\sqrt{\frac{T_i M_e}{T_e M_i}} + R_e \overline{c}_{Te}\right), \quad (7)$$

where $\overline{B} = [c/(eB_p v_{ti})](p_e'/n_e + \mu_{2e}T_e'/\mu_{1e})$, $\overline{c}_{pa} = cp_a'/(n_a|e_a|B_p v_{ta})$, and $\overline{c}_{Ta} = cT_a'/(n_a|e_a|B_p v_{ta})$ [23]. The nonlinearity that is responsible for the bifurcation is in μ_{1i} which has a local maximum at a certain value of U_{pm}. Because parallel flow is usually subsonic, i.e., $|V_\parallel/v_{ti}| \ll 1$, we neglect the difference between U_{pm} and M_p. This approximation decouples parallel flow $V_\parallel$ and radial electric field. Equation (7) becomes approximately a nonlinear equation for E_r or M_p. In general, of course, we need to solve coupled equations for $V_\parallel$ and M_p.

Equation (7) is solved numerically by plotting the left- and right-hand sides of it versus U_{pm}. The solutions are the intersections of these two curves. We use the ERS-mode-like parameters: $B = 3$ T, $R = 2.6$ m, $a = 0.8$ m, $\epsilon = 0.1$, $N = 20$, $q = 2.5$, and $\delta = 1.3 \times 10^{-3}$. The bifurcation process is demonstrated in Fig. 1. The gradient parameters are fixed to be $\overline{c}_{Te} = \overline{c}_{pe} = 0$. $\overline{B} = [0.85 + (\mu_{2e}/\mu_{1e})0.85]$, $\overline{c}_{pi} = 0.85$, $\overline{c}_{Ti} = 0.85$, $\overline{c}_{pH} = 2.0$, and $\overline{c}_{TH} = 0$. The L-mode solution is described by the intersection of the solid curve [the left side of Eq. (7)] and the solid line with crosses [the right side of Eq. (7)] for 4 keV ions as shown in Fig. 1. When the hot particle density increases to 2.4×10^{12} cm^{-3}, which is 10% of the thermal density, there are multiple solutions as can be seen from the intersections between the solid curve and the solid line with squares in Fig. 1. The solution in the middle is unstable. The solution with the largest value of U_{pm} is the ERS-mode solution. When ion temperature increases to 6 keV, only the ERS-mode solution exists as indicated by the intersection between the dotted curve and the dotted line. Once in the ERS state, particle confinement improves because turbulence fluctuations are suppressed by the gradients of $\mathbf{E} \times \mathbf{B}$ and diamagnetic angular velocity, and thermal particle density increases. The increased thermal particle density tends to reduce neutral particle penetration and, therefore, hot particle density. When the hot particle density decreases from 2.4×10^{12} cm^{-3} to 1.2×10^{12} cm^{-3} (solid line), and finally to zero (dotted line), the radial electric field relaxes, as shown in Fig. 2. Note also in the relaxation process there is no back bifurcation. This is because the slope of the nonlinear viscosity in the large U_{pm} region changes in the higher ion temperature regime. Interestingly, no bifurcation process is observed in TFTR in the relaxation phase either.

The time scale involved in the bifurcation can be crudely estimated from the characteristic damping frequency of the equation and the rate of the change of the control parameters, i.e., T_i in our example. The characteristic poloidal flow damping frequency is of the order of ν_{ii}/ϵ^x [24–26]. Here, x is a number between 0 to 1. The rate of change of the control parameters depends on the heating rate. If the heating rate is extremely slow so that ion temperature approaches the critical value adiabatically, the bifurcation time is at first of the order the linear damping rate, i.e., $(\nu_{ii}/\epsilon^x)^{-1}$ and then, as T_i approaches the critical value, the time scale slows down.

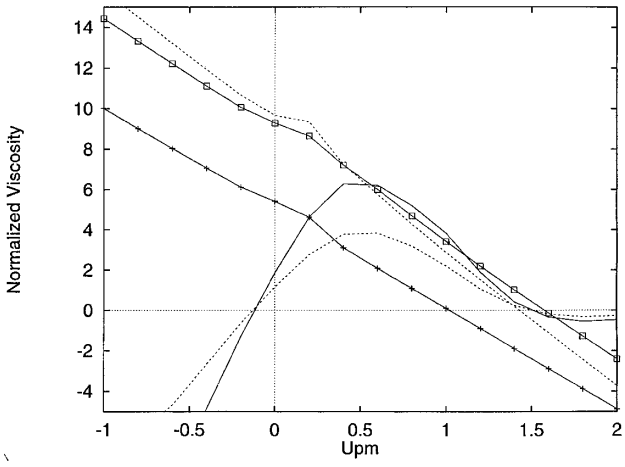

FIG. 1. An example of the bifurcation processes. The L-mode solution is the intersection of the solid curve and solid line with crosses for 4 keV ions. As hot particle density increases to 2.4×10^{12} cm^{-3}, there are multiple solutions, as indicated by the intersections of the solid curve and solid line with squares. The solution in the middle is unstable. The new stable solution is the ERS-mode solution. When ion temperature increases to 6 keV, only the ERS-mode solution exists, as indicated by the intersection between the dotted curve and the dotted line.

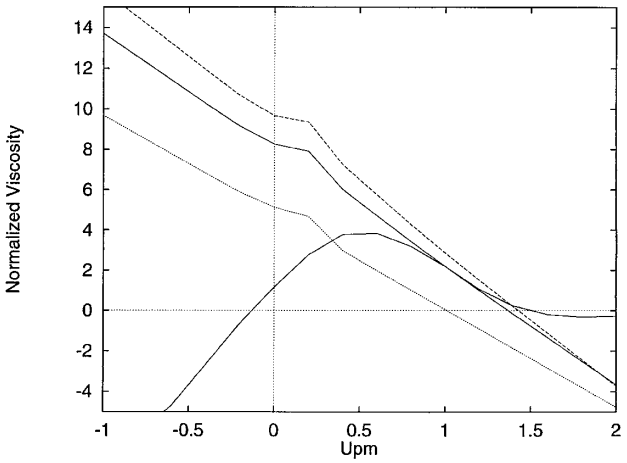

FIG. 2. An example of the relaxation processes. As the hot particle density decreases after the bifurcation from 2.5×10^{12} cm^{-3} to 1.2×10^{12} cm^{-3} (solid line), and finally to zero (dotted line), the value of E_r decreases to a L-mode-like value.

This is the well-known critical slowing down phenomenon [27,28]. However, if T_i changes at a rate faster than the critical slowing down rate, the critical slowing down rate will not be observed. The bifurcation rate is then controlled by $(\nu_{ii}/\epsilon^x)^{-1}$, nonlinearity of the system, and the heating rate. Note that $(\nu_{ii}/\epsilon^x)^{-1}$ in the parameters of interest is about 20 ms for $x = 0$, well within the experimentally observed time scale in TFTR which is about 20–40 ms [10]. The bifurcation time scale is therefore in good agreement with experimental observations.

The relaxation time scale is of the order of the transport time scale to allow plasma density to build up. This is again consistent with the observation.

The theory presented here requires a value of the toroidal magnetic field ripple strength of the order of 10^{-3}. In the NCS-mode plasmas [9], ripple strength is said to be much smaller than this value. It is difficult in NCS plasmas to observe the ERS-mode-like bifurcation.

We emphasize that the scenario employed to demonstrate the bifurcation and relaxation processes shown in Figs. 1 and 2 is not unique. One could, for example, let gradient parameters $\overline{c}_{pa}$ and $\overline{c}_{pT}$ evolve during the bifurcation and the relaxation processes as in the experiments. Here, we are interested only in demonstrating the fundamental physics mechanism. The detailed time-dependent transport simulation will be presented later.

In conclusion, we have demonstrated a bifurcation and relaxation mechanism for the radial electric field with ERS-like plasma parameters by including the ripple loss of both thermal and hot particles. Hot particle ripple loss assists bifurcation. After bifurcation, the hot particle density reduces due to improved confinement, and E_r relaxes. During the relaxation process, no back bifurcation is observed in the regime of interest. This mechanism could be responsible for the evolution of E_r observed in TFTR ERS mode.

The authors thank R. E. Bell and R. Nazikian for useful discussions.

[1] ASDEX Team, Nucl. Fusion **29**, 1959 (1989).
[2] F. Wagner *et al.*, Plasma Phys. Controlled Fusion **36**, A61 (1994).
[3] K. Toi *et al.*, in *Plasma Physics and Controlled Nuclear Fusion Research 1994* (International Atomic Energy Agency, Vienna, 1994), Vol. 2, p. 331.
[4] K. C. Shaing and E. C. Crume, Jr., Phys. Rev. Lett. **63**, 2369 (1989).
[5] S.-I. Itoh and K. Itoh, Phys. Rev. Lett. **60**, 2376 (1988).
[6] K. Ida *et al.*, Phys. Rev. Lett. **65**, 1364 (1990).
[7] F. M. Levinton, M. C. Zarnstorff, S. H. Batha, M. Bell, R. E. Bell, R. V. Budny, C. E. Bush, Z. Chang, E. D. Fredrickson, A. Janos, J. Manickan, S. T. Ramsey, G. L. Schmidt, E. J. Synakowski, and G. Taylor, Phys. Rev. Lett. **75**, 4417 (1995).
[8] S. Ishida *et al.*, Phys. Rev. Lett. **79**, 3917 (1997).
[9] E. J. Strait *et al.*, Phys. Rev. Lett. **75**, 421 (1995).
[10] R. E. Bell, F. M. Levinton, S. H. Batha, E. J. Synakowski, and M. C. Zarnstorff, Phys. Rev. Lett. **81**, 1429 (1998).
[11] S. de Pena Hempel, H. Meister, A. Kallenbach, A. Peeters, and ASDEX Upgrade Team, in *Proceedings of the 25th European Physical Society Conference on Controlled Fusion and Plasma Physics, 1998* (European Physical Society, Prague, 1998), p. 484.
[12] K. C. Shaing, A. Y. Aydemir, W. A. Houlberg, and M. C. Zarnstorff, Phys. Rev. Lett. **80**, 5353 (1998).
[13] T. E. Stringer, Plasma Phys. **16**, 12 (1972).
[14] J. N. Davidson, Nucl. Fusion **16**, 731 (1976).
[15] K. T. Tsang, Nucl. Fusion **17**, 557 (1977).
[16] A. H. Boozer, Phys. Fluids **23**, 2283 (1980).
[17] R. J. Goldston, R. B. White, and A. H. Boozer, Phys. Rev. Lett. **47**, 647 (1981).
[18] U. Stroth *et al.*, Plasma Phys. Controlled Fusion **40**, 1551 (1998).
[19] For a review, see P. N. Yushmanov, in *Review of Plasma Physics*, edited by B. B. Kadomtsev (Consultants Bureau, New York, 1990), p. 117.
[20] K. C. Shaing and J. D. Callen, Phys. Fluids **26**, 3315 (1983).
[21] K. C. Shaing, Phys. Fluids B **2**, 2847 (1990).
[22] S. P. Hirshman and D. J. Sigmar, Nucl. Fusion **21**, 1097 (1981).
[23] The exact expressions for D_i, D_H, and D_e can be found by comparing Eq. (7) with Eq. (2) after Eqs. (3)–(6) are inserted, for example, $D_i = -[(\Gamma_t^i + \Gamma_b^i + \Gamma_{rp}^i)eB_p/(cn_iM_e\mu_1^e\nu_{ti})]/(\overline{c}_{pi} + M_p + R_i\overline{c}_{Ti})$. The expressions for D_H and D_e are similar to D_i except the species-dependent parameters are changed accordingly.
[24] C. T. Hsu, K. C. Shaing, and R. Gormley, Phys. Plasmas **1**, 132 (1994).
[25] R. C. Morris, M. G. Haines, and R. J. Hastie, Phys. Plasmas **3**, 4513 (1996).
[26] S. V. Novakovskii, C. S. Liu, R. Z. Sagdeev, and M. N. Rosenbluth, Phys. Plasmas **4**, 4272 (1997).
[27] S. K. Ma, *Modern Theory of Critical Phenomenon* (Benjamin, Reading, MA, 1976).
[28] K. C. Shain, Phys. Fluids **27**, 1924 (1984).